JOURNAL OF PROPULSION AND POWER
Vol. 15, No. 3, May–June 1999

Performance Evaluation of Scramjet Combustors Using Kinetic Energy and Combustion Efficiencies

Goro Masuya,* Tomokazu Uemoto,† and Yoshihiro Wakana‡
Tohoku University, Sendai, Miyagi 980-8579, Japan
and
Kenji Kudou,§ Atsuo Murakami,§ and Tomoyuki Komuro§
National Aerospace Laboratory, Kakuda, Miyagi 981-1525, Japan

A performance parameter of scramjet combustors was introduced on the basis of thrust. It was written in terms of the kinetic energy and combustion efficiencies. To evaluate this parameter from available data of direct connect combustor experiments, ideal nozzle calculation was carried out for each stream tube, starting from the data at the combustor exit, and the results were integrated across the nozzle exit to obtain the efficiencies and performance parameter. The relative importance of heat release and aerothermodynamic losses were compared for various configurations of the fuel injectors and combustor ducts. For flight Mach numbers less than 7, the heat release had a stronger influence on the performance than the losses. The optimum length, where the effects of both effects canceled each other, was 15–20 times the flow section width for the rectangular section combustor with perpendicular wall injectors.

Nomenclature

C_C = nondimensional heat of combustion
C_F = nondimensional static enthalpy addition by fuel
d_j = diameter of fuel-injection orifice
f = fuel–air ratio
G = gap width of combustor duct entrance
H = height of combustor duct entrance
h = specific enthalpy
I_{sp} = specific impulse
K_C = normalized form of K_C^*, see Eq. (4)
K_C^* = scramjet combustor performance parameter
L = length
M = Mach number
p = pressure
R = leading-edge radius of strut
T = temperature
V = velocity
α = fuel-injection angle
γ = specific heat ratio
η = efficiency
θ = wedge half-angle of strut
κ = nondimensional kinetic energy
Λ = sweep angle of step
φ = fuel-equivalence ratio
ψ = nondimensional specific enthalpy at inlet exit

Subscripts

C = combustor or combustion
e = exit
I = inlet
i = entrance
ise = isentropically expanded
KE = kinetic energy
mix = mixing
N = nozzle
PT = stagnation pressure recovery
per = perpendicular injection
t = stagnation condition
total = total fuel
1 = constant-area section downstream of step
∞ = flight condition

Received Sept. 2, 1997; revision received Aug. 22, 1998; accepted for publication Sept. 14, 1998.

*Professor, Department of Aeronautics and Space Engineering. Member AIAA.
†Graduate Student, Department of Aeronautics and Space Engineering; currently at Ishikawajima–Harima Heavy Industries Company, Ltd.
‡Graduate Student, Department of Aeronautics and Space Engineering; currently at Toyota Motors Company, Ltd.
§Senior Researcher, Kakuda Research Center, Ramjet Propulsion Research Division.

Introduction

IN jet-propulsion engines, which produce thrust mainly by reaction of gas or fluid ejection, a large part of combustion's heat is converted into the kinetic energy of exhausts to produce propulsive work. In a hypersonic air-breathing engine, such as a scramjet engine or a combined cycle engine, the kinetic energy of an incoming airstream becomes the same order with the heat of combustion in the engine. Therefore, the aerothermodynamic loss of available energy, which can be converted into kinetic energy in high-speed engines, such as a scramjet or a combined cycle engine, may cause a serious decrease of thrust. It is therefore important to evaluate the gain and loss of available energy for various flow duct geometry and fuel-injection configurations of engines.

Thrust delivered by the engine is one of the most suitable indexes to evaluate the design of engine configurations. However, because of extreme conditions and high costs required for measuring the thrust in ground or flight tests of a whole scramjet engine, most experimental studies are conducted in each component level where the direct measurement of engine thrust is not possible. Among the components of the scramjet, the combustor is the most complicated one, where fuel injection, mixing, and combustion occur. Heat addition and various losses simultaneously occur in the combustor, and they are closely related to each other in several ways, for example, entropy increase by heat addition to finite Mach number flow,[1] dissipation of intense turbulence required for good mixing,[2] larger wall friction loss caused by a longer combustor for complete combustion, etc.

In supersonic-combustor experiments, performances have usually been measured by such parameters as mixing efficiency, η_{mix}, combustion efficiency, η_C, and/or stagnation pressure recovery efficiency, η_{PT}. However, each shows only a facet of the whole

combustor performance. For example, η_C shows how well the combustion and heat release are achieved, but it indicates nothing about the aerodynamic loss. Though η_{PT} is a familiar index of the aerodynamic loss in subsonic and low-supersonic flows, it becomes difficult to use in the hypersonic range for two reasons: 1) real-gas effects, which are significant in this range, make it difficult to calculate the stagnation conditions; and 2) logarithmic relations between the stagnation pressure and the entropy cause a great change in the useful range of η_{PT} with flight Mach number, M_∞. In the subsonic flight regime, ramjets can deliver positive thrust only when η_{PT} is near unity, whereas the thrust of a scramjet operating at a very high M_∞ remains positive, even if η_{PT} is < 0.01. Therefore, it is better to replace η_{PT} with one that more suitably represents the aerothermodynamic losses. Among the various efficiencies,[3] the kinetic energy efficiency, η_{KE}, would be suitable to evaluate the losses in the ramjet/scramjet engine.[4,5] Mager defined nonadiabatic form of η_{KE} as follows[4]:

$$\eta_{KE} = \frac{V_{ise}^2/2h_{te}}{V_{isi}^2/2h_{ti}} \tag{1}$$

where V_{ise} is the velocity obtained by isentropic expansion to the atmospheric pressure p_∞, h_t is the specific stagnation enthalpy, and i and e denote the entrance and exit conditions, respectively. Equation (1) is applicable to the whole engine as well as its components. When the efficiency is applied for the whole engine, it is denoted as η_{KEng} in the present paper.

Curran et al.[4] compiled I_{sp} data of various hydrocarbon-fueled subsonic combustion ramjets, and showed that these data were well correlated with a curve for $\eta_{KEng} = 0.64$ and $\eta_C = 1$. For scramjet engines, they argued on the applicability of η_{KE}, because the airstream in the scramjet engine was not decelerated to a certain reference Mach number. In addition, they found only a few I_{sp} data for the scramjet engines. However, they suggested that those limited data for hydrogen-fueled scramjet tested at a M_∞ of 3–6.5 might be fairly correlated with $\eta_{KEng} = 0.7$ and $\eta_C = 1$, as shown in Fig. 1. Note that in the present paper, I_{sp} is defined as the ratio of thrust to fuel mass flow rate, and its unit is not in seconds but in m/s. Although the assumption of $\eta_C = 1$ may be favorable for subsonic combustion ramjets, it is difficult to realize in scramjet engines. Actually, η_C of 0.7 was reported in a compiled experiment.[6] For a lower value of η_C, a higher η_{KEng} than that suggested by Curran,[4] is required to match the prediction curve with the same I_{sp} data. If $\eta_C = 0.7$, the data would be well correlated with $\eta_{KEng} = 0.8$. As shown in Fig. 1, if

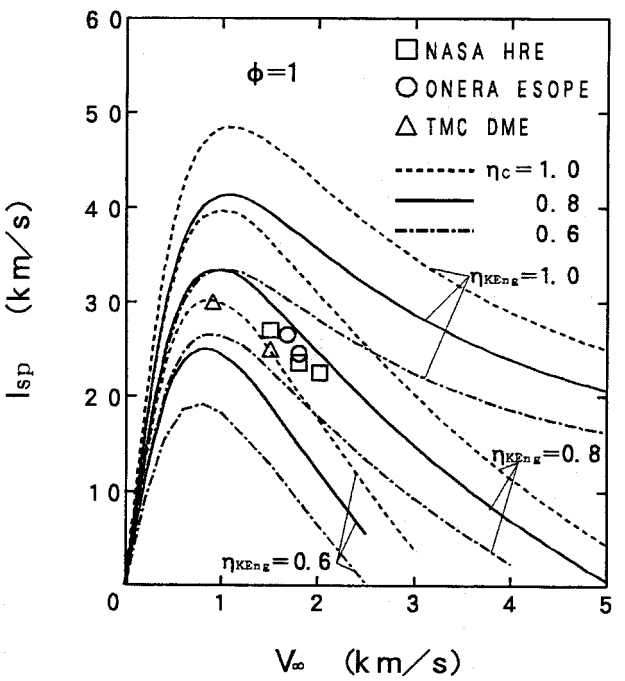

Fig. 1 Specific impulse of scramjet for various values of η_{KEng} and η_C.

the values of η_{KEng} and η_C do not change with M_∞, the set of higher η_{KEng} and lower η_C results in higher I_{sp} in the high M_∞ range, than that in the set of lower η_{KEng} and higher η_C. We found very few experimental results of supersonic combustors that included both η_{KE} and η_C, or their equivalent quantities.[7] Thus, it is important to compile further data about these efficiencies for the scramjet combustors, and to evaluate them with a single performance parameter closely related to thrust.

Energy efficiency[8] and thrust potential[9,10] were proposed as engine performance parameters. Riggins[11] compared them and showed that the latter is more suitable than the former for evaluating the scramjet combustor performance. Another combustor performance parameter related to the thrust was derived in terms of η_{KE} and η_C by one of the present authors.[5] This parameter, as well as the thrust potential, are calculated from the available thrust for a specified engine exit condition such as the cross-sectional area[9–11] or the pressure.[5,9–11] In the present study, the specified condition at the engine exit was the pressure, and it was set equal to that of the atmosphere at the simulated flight altitude. Note that this condition may not maximize the thrust because of increased pressure drag on the external surface of the engine or the vehicle where the scramjet engine is integrated. However, an accurate evaluation of such drag that may depend on the total vehicle design, is out of the scope of the present paper, and we adopt the condition of the atmospheric nozzle exit pressure in the present paper. As shown in the next section, the combustor performance parameter is constructed only by the terms related to the combustor design in the equation for the thrust, whereas the thrust potential is based on the thrust itself.[9] Thus, close examination of the combustor performance parameter would give us insight on the contribution of gain and loss of the available energy to thrust production.

The purpose of the present paper is first to calculate the combustor kinetic energy efficiency, η_{KEC}, as well as the combustion efficiency, η_C, from the existing experiments, of which detailed data were available, and to then evaluate the combustor performance parameter from them and discuss the effects of various factors on the parameter.

Scramjet Combustor Performance Parameter

The performance of the engine component should be related to that of the whole engine, such as the thrust or the specific impulse, I_{sp}. For the ram/scramjet engine with the pressure at the nozzle exit equal to the atmospheric pressure, I_{sp} can be expressed in term of η_{KEng} and η_C, as follows.[5] Drag of the engine external surface would be counted as a part of the vehicle drag

$$I_{sp} = \frac{V_\infty}{f}\left\{\left[(1+f)\eta_{KEng}\left(\frac{\eta_C C_C + C_F}{1+\kappa_\infty}+1\right)\right]^{\frac{1}{2}} - 1\right\} \tag{2}$$

where V_∞ is a flight speed, f a fuel–air ratio; C_C a nondimensional heat of combustion to a unit mass of air; C_F a nondimensional fuel enthalpy at the injector manifold to a unit mass of air; and $\kappa_\infty \equiv (\gamma_\infty - 1)M_\infty^2/2$, a nondimensional specific flight kinetic energy. Energy, heat, and enthalpy are nondimensionalized by the atmospheric static enthalpy at the flight condition.

Because the kinetic energy efficiency of the whole engine, η_{KEng}, is a product of those of all engine components, we find three combustor-related variables in Eq. (2), namely, f, η_{KEC}, and η_C, which represent the effects of mass addition, losses, and heat release, respectively. The combustor performance may be evaluated by these three terms. However, the fuel–air ratio is mostly determined by consideration of a total propulsion system such as the thrust level necessary for the mission of the vehicle or the cooling requirement, and f is not influenced by the combustor design. Thus, it is better that the combustor performance is evaluated by a parameter K_C^*, defined[5] by the following equation, which includes only η_{KEC} and η_C:

$$K_C^* = \eta_{KEC}\left(\frac{\eta_C C_C + C_F}{1+\kappa_\infty}+1\right) \tag{3}$$

Note that the effect of the fuel momentum is included in η_{KEC}.

Table 1 Combustor configuration and experimental conditions

Model number	G, mm	H, mm	L_1, mm	L_C, mm	Injector type	α, deg	Λ, deg	d_j, mm	R, mm	θ, deg	φ_{total}	T_{tCi}, K
I	32	147.3	96	138–1056	Wall N1	90	0	4.0/2.8	—	—	1.0	2000
	↑	↑	96/22	↑	Wall N2	↑	↑	↑	↑	↑	↑	↑
	↑	↑	22	262–982	Wall N3	↑	↑	↑	↑	↑	↑	↑
	↑	↑	96	138–1056	Wall S1	↑	45	↑	↑	↑	↑	↑
	↑	↑	96	↑	Wall S2	↑	±45	↑	↑	↑	↑	↑
II	20	94.3	28	360	Strut A	0/90	0	2.5	1.0	6	0.4	1500
	↑	↑	↑	↑	Strut E	↑	↑	↑	1.5	7	↑	↑

To normalize K_C^*, we need an ideal value of each parameter in Eq. (3). Though the ideal heat release can be readily represented by η_C of unity, it is difficult to specify loss caused by heat addition in a finite Mach number stream (Rayleigh loss), because real combustion occurs neither in a constant-area duct nor under a constant-pressure condition. However, if the airstream is completely diffused to a Mach number of zero in the inlet, η_{KEC} does not reduce with any amount of heat addition. Therefore, normalized K_C^*, denoted as K_C, is defined as follows, and is used for evaluation of the combustor performance in the present study:

$$K_C = \eta_{\text{KEC}}\left(\frac{\eta_C C_C + C_F + 1 + \kappa_\infty}{C_C + C_F + 1 + \kappa_\infty}\right) \tag{4}$$

This equation shows that K_C is proportional to η_{KEC}, whereas η_C affects only a fraction of $C_C/(C_C + C_F + 1 + \kappa_\infty)$. This portion diminishes as the flight Mach number increases.

K_C can be related to the thrust potential or the specific thrust if it is estimated for the same exit condition as for K_C. The specific thrust is fI_{sp}, then we have the following relation:

$$\text{Thrust Potential} = V_\infty\left\{\left[(1+f)K_C\left(\frac{C_C + C_F}{1+\kappa_\infty} + 1\right)\right]^{\frac{1}{2}} - 1\right\} \tag{5}$$

Experiments

In this section, the experiments[12–14] that provide the data used in the present study are briefly reviewed. Two rectangular cross-sectional supersonic combustor models, no. I (Refs. 12 and 13) and no. II (Ref. 14), were tested with the direct-connect hydrogen vitiation air heater[15] at the National Aerospace Laboratory, Kakuda Research Center. Spatial nonuniformity of gas compositions at the exit of the vitiation heater was less than ±5% of the averaged value calculated from the flow rates of the supplied gases.[15] The combustors with the facility nozzles are shown in Fig. 2, and the major dimensions of the combustors and the experimental conditions are indicated in Table 1. The Mach number of the airstream at the combustor inlet, M_{Ci}, was 2.5. The nominal value of the stagnation pressure of the airstream there, p_{tCi}, was 1.0 MPa. The nominal stagnation temperature, T_{tCi}, of combustor no. I was 2000 K. To avoid a severe thermal load to the strut, tests of combustor no. II were carried out at lower stagnation temperature of 1500 K. The stagnation temperature was not measured, but calculated, from the flow rates of the gases supplied to the vitiation heater, assuming the chemical equilibrium without heat loss. The specific heat ratio of the vitiated air at the entrance of the combustor, γ_{Ci}, was calculated as 1.305 for combustor no. I and 1.343 for combuster no. II. The experimental conditions of each run were within ±5% of their nominal values.

The entrance section of combustor no. I was 32 mm in width (G) and 147.3 mm in height (H). Fuel was perpendicularly injected from circular orifices $0.4G$ downstream a backward-facing step of $0.1G$ height on each side wall. There were four injection orifices on one of the side walls and five on the other, and they were located in staggered positions to each other. The injector orifice diameter d_j was $G/8$ for all of four orifices on one side wall and three central orifices of the other side wall, whereas that of the two outer orifices

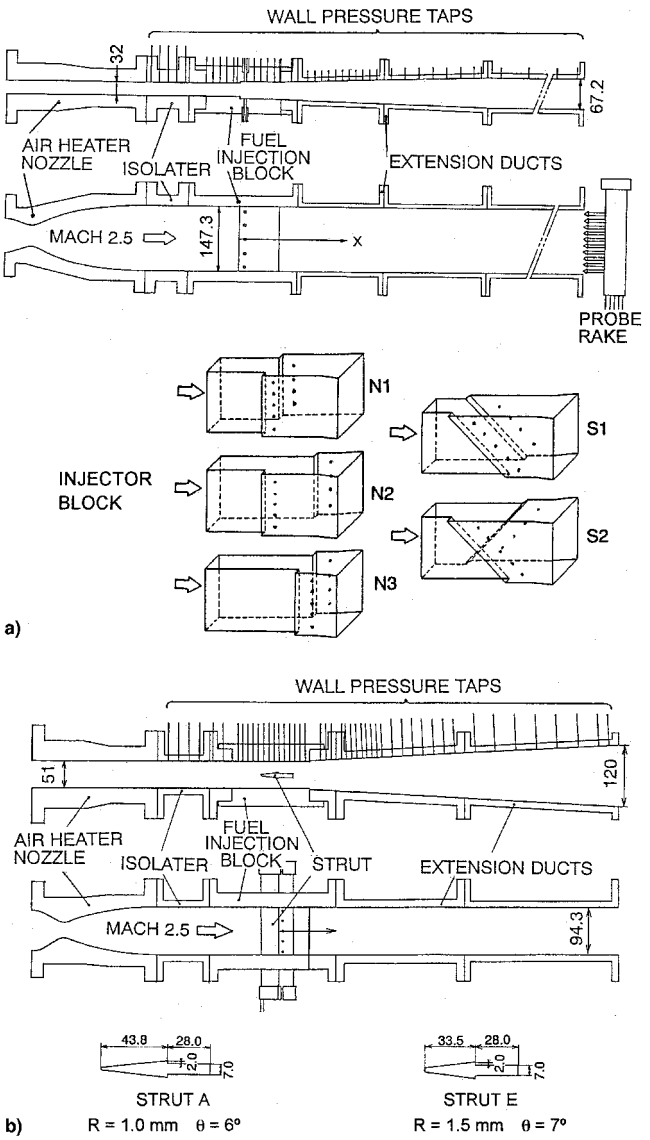

Fig. 2 Experimental setup (all dimensions in mm): a) combustor no. I (wall injection)[12,13] and b) combustor no. II (strut injection).[14]

was $3G/40$. The lateral spacing of the orifices was G. There were five different injector patterns, N1, N2, N3, S1, and S2, with the sweep angle of the step, Λ, and the length of constant-area region behind the step, L_1, as shown in Fig. 2a and Table 1.

In combustor no. II, there was a fuel-injection strut in the midplane. Each flow path was 20 mm in width (G) and 94.3 mm in height (H). The cross-sectional shapes of struts A and E, with a different leading-edge radius, R, and wedge half-angle, θ, are shown in Fig. 2b. Fuel was injected perpendicular and/or parallel to the airstream from the orifices on both sides and/or the base of the strut, respectively. Five perpendicular injection orifices of $G/8$ diameter

were located $0.4G$ downstream of the backward-facing step of $0.1G$ height on the strut. Four parallel injection orifices of the same diameter were at the staggered locations with the perpendicular injection orifices.

The combustion ducts downstream of the fuel injector were constructed from removable extension ducts to change the combustor length, L_C. The extension ducts were divergent to downstream, except the most downstream duct of combustor no. I, which had a constant cross section to avoid separation at the exit. The walls of the combustors, as well as those of the air heater and its nozzle, were not actively cooled, and the duration of each run was 7 s.

Wall pressure distributions were measured by mechanical pressure scanners. End-to-end error of the pressure measurement system, including a pressure transducer, a signal conditioner, a dc amplifier, and an A/D converter, was less than ±0.5% of the full range of the transducer. Pitot pressure and dry gas compositions in each exit section were measured at 70 and 80 points for combustors no. I and II, respectively, using a water-cooled 10-point pitot pressure/gas sampling probe rake. The orifice diameter of the probe was 0.7 mm. Sample gas was analyzed by a gas chromatography with a molecular sieve 5A column to obtain a stable dry composition. The static pressure of each survey point in the exit section was interpolated from the wall pressures of both side walls. From the survey data and measured gas flow rates, local flow properties such as equilibrium gas composition, Mach number, and stagnation conditions were calculated.[12] Typical wall pressure distributions and cross-sectional local equivalence ratio distributions of combustor no. I with injector S2 are shown in Figs. 3 and 4, respectively. Further details, including additional experimental data of combustors no. I and II are presented in Refs. 12–14.

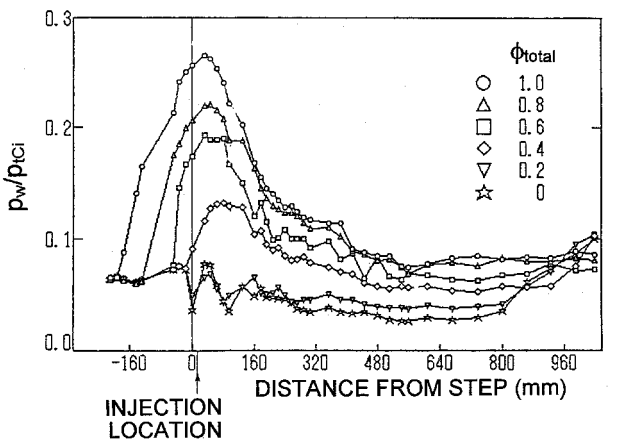

Fig. 3 Typical wall pressure distributions (combustor no. I, injector S2).

Mitani et al. analyzed[16] and experimentally verified[17] the effect of the probe configuration on freezing of the reaction in the gas-sampling system for the scramjet engines. According to the results of Ref. 17, the reaction of certain conditions could not be completely frozen in the sampling probes used in the present experiments. Therefore, note that the combustion efficiencies of the present study might be somewhat overestimated. Their experiment[17] was conducted using combustor no. II without the strut, and the fuel was injected from the wall. The largest difference between the combustion efficiencies obtained by the probe used in the experiments[12–14] and analyzed in the present study and one[17] in which the sample gas was well quenched was observed for T_{tCi} of ~1200 K. The differences of the η_C for $T_{tCi} > 1500$ K were 5% or less.[16,17]

Calculation of Performance Parameters

Flight Conditions

Because the thrust performance evaluation required the flight atmospheric conditions simulated in the experiment, they were estimated from the conditions at the combustor entrance. To simplify and clarify the calculation process, the constant atmospheric temperature T_∞ of 240 K and adiabatic flow in the inlet were assumed. Using the adiabatic relation with the values of T_{tCi}, T_∞, and γ_{Ci}, the flight Mach number M_∞ was calculated to be 6.93 for combustor no. I and 5.54 for combustor no. II. Then the flight stagnation pressure, $p_{t\infty}$, for the assumed value of η_{KEI} was calculated using the relation[3] between η_{KE} and η_{PT}, with M_∞, γ_{Ci}, and p_{tCi}. η_{KEI} was used to represent the inlet performance because its value was needed in calculating η_{KEC} from η_{KEng}. The atmospheric pressure p_∞ was obtained from the isentropic relation with $p_{t\infty}$ and γ_{Ci}. For the change of η_{KEI} from 0.9 to 1.0, the inlet compression ratio, p_{Ci}/p_∞, changes from 47 to 494 for combustor no. I with $M_\infty = 6.93$, or from 14.5 to 76.3 for combustor no. II with $M_\infty = 5.54$.

In this calculation, γ_{Ci} was used instead of γ_∞ for the pure air because the conditions obtained from γ_∞ should result in an inconsistency in the case of $\varphi = 0$ and $L_C/G = 0$. In addition to this inconsistency, the choice of the specific heat ratio for estimating the flight condition results in considerably different performances. If we had used the specific heat ratio of pure air, i.e., 1.4, then M_∞ and p_{Ci}/p_∞ for $\eta_{KEI} = 1.0$ would have been 6.06 and 98 for combustion no. I, and 5.12 and 35.6 for combustion no. II, respectively. Expansion of the exhaust in the nozzle would be quite restricted for these cases, and the resulting η_{KEC} would be lower than those shown in the present study.

Ideal Nozzle Calculation

The measured distributions at each combustor exit section were used as the initial values of the ideal nozzle calculation. The data at

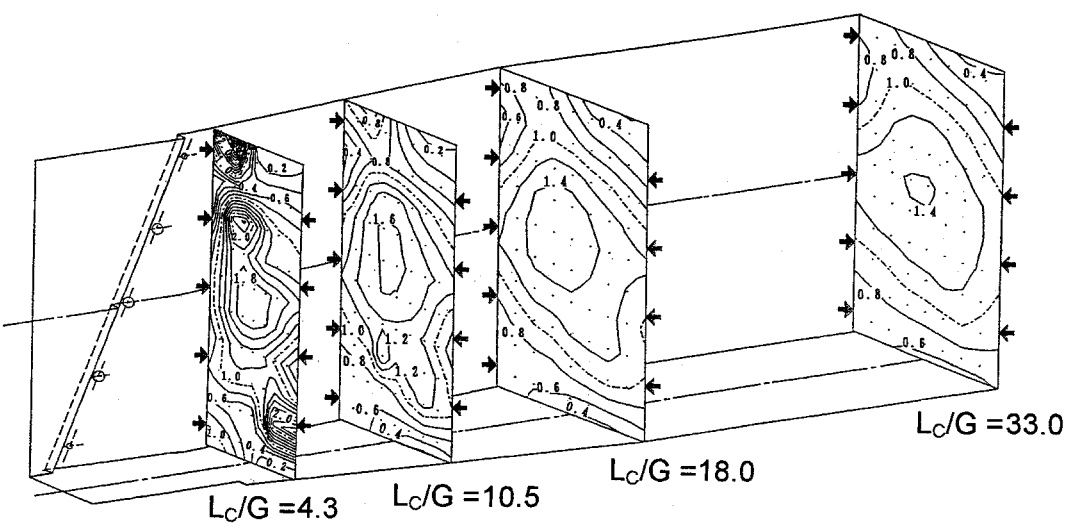

Fig. 4 Typical equivalence ratio distributions (combustor no. I, injector S2).

each probe position were considered to represent those of a stream tube around the point. The properties of each stream tube at the nozzle exit were numerically calculated by the quasi-one-dimensional equations[1] with the equilibrium chemistry. Because we concentrate on the combustor performance, each stream tube was assumed to expand isentropically from the combustor exit pressure, p_{Ce}, to p_∞, without further mixing and combustion. Friction and heat transfer on the nozzle wall were also ignored.

The calculated properties of each stream tube at the ideal nozzle exit were numerically integrated to obtain averaged values. Data at the points closest to the combustor duct walls were corrected for boundary-layer effects, assuming a one-seventh power-law velocity distribution and the modified Crocco's energy distribution.[18] The recovery factor for the wall temperature was set as 0.2, based on the experimental results.[13]

Combustion Efficiency

The combustion efficiency used in Eqs. (2–4) is based on the heat release, whereas those indicated in Ref. 6 and Refs. 12–14 were defined as the ratio of burned to combustible fuel flow rate at the combustor exit. In the present calculation, the difference between the stagnation enthalpy flow rates at the nozzle exit and the combustor entrance was compared with the heat of combustion of hydrogen, namely, 120 MJ/kg multiplied by the fuel flow rate.

Results and Discussion

Effects of Inlet Kinetic Energy Efficiency

Initially, the influence of change in an assumed value of the inlet kinetic energy efficiency, η_{KEI}, was checked by the results of combustor no. I with injector N1 and $L_C/G = 10.5$. Figure 5 shows the change of η_{KEC} and K_C with η_{KEI}. Experimental conditions for combustor no. I corresponded to M_∞ of 6.93, and the inlet compression ratio of 275 for $\eta_{KEI} = 0.98$. For the specified values of M_∞, p_{Ci}, and p_{Ce}, higher η_{KEI} corresponds to lower p_∞, resulting in higher $V_{ise\,i}$ and $V_{ise\,e}$. Thus, it is not easy to say whether η_{KEC} increases with η_{KEI} or not from the formula. The present results indicate that η_{KEC} almost linearly increases from 0.93 to 0.96 as η_{KEI} increases from 0.94 to 0.99. These values of η_{KEC} seem very encouraging because they result in η_{KEng} that is more than 0.835 for the product, and $\eta_{KEI}\eta_{KEN}$ that is more than 0.90.

If we assume constant-pressure combustion, η_{KEC} was expressed as follows[5]:

$$\eta_{KEC} = \frac{1+\kappa_\infty}{\eta_{KEI}\kappa_\infty}\left\{1-\left[1-\frac{(1+\kappa_\infty-\psi)\omega}{1+\kappa_\infty+\eta_C C_C + C_F}\right]\right.$$
$$\left.\times\left[\frac{1+(1-\eta_{KEI})\kappa_\infty}{\psi}\right]\right\} \qquad (6)$$

where ψ is the nondimensional static enthalpy at the inlet exit, and ω is a variable including the effects of axial injection velocity of fuel and drag of the combustor. For the change of η_{KEI}, the present result behaves similarly to Eq. (6).

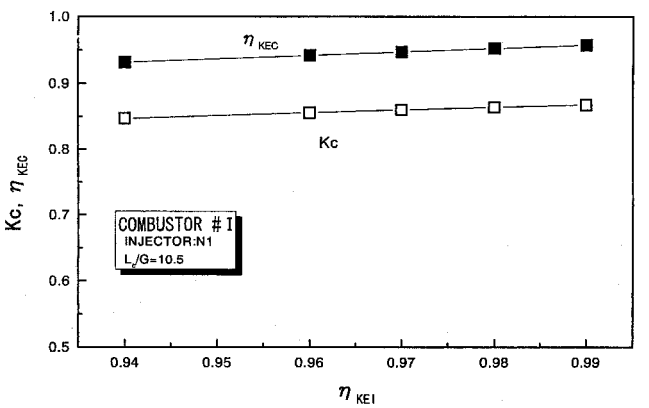

Fig. 5 Effects of η_{KEI} on combustor performances (combustor no. I).

Effects of Combustor Length

Effects of L_C/G on η_C, η_{KEC}, and K_C are shown in Fig. 6 for combustor no. I. The value of η_{KEI} was fixed at 0.98. As expected, η_C for injector S2, for example, increases from 0.72 to 0.91 as L_C/G increases from 4.3 to 33, whereas η_{KEC} decreases from 0.945 to 0.930. K_C changes from 0.79 to 0.88. The trend of K_C is close to that of η_C, because C_C is about 12 and is higher than κ_∞ of about 7.3. In addition, the change of η_{KEC} was less than one-tenth of the change of η_C. However, for $L_C/G \geq 18$, K_C was almost constant or even slightly decreased with the length. In this part of the combustor, about a 1.7% increment of η_C was canceled by a 1.3% decrement of η_{KEC}. We find that the optimum value of L_C/G was about 15–20 for all of the injectors of combustor no. I tested in the present experiment. This optimum L_C/G is about one-half of L_C/G for the sufficient mixing of fuel perpendicularly injected from the walls.[19] Further extension of the duct increases only the engine weight and cooling requirement. If the penalty of the weight and/or the cooling requirement is very severe, L_C/G less than 15 could be selected. When M_∞ becomes considerably higher than the present experimental condition,

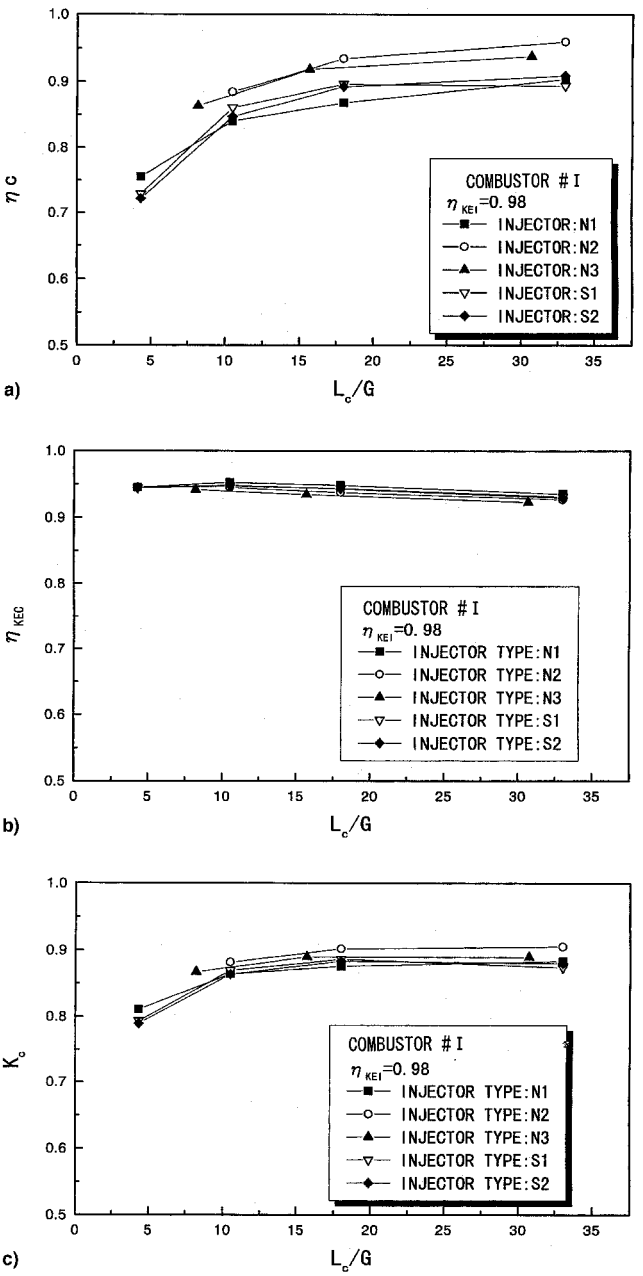

Fig. 6 Effects of combustor length on scramjet combustor performances (combustor no. I): a) η_C, b) η_{KEC}, and c) K_C.

K_C would be much less influenced by η_C and the optimum length would become shorter.

As mentioned previously, η_C, shown in Fig. 6a, might be overestimated because of incomplete freezing of the reaction in the gas-sampling probes used in this study. Thus, it is interesting to compare η_C calculated from the wall pressure distribution shown in Fig. 3 with a quasi-one-dimensional theory. Such a calculation was carried out by Murakami et al.,[13] assuming constant gas properties. Their calculated values of η_C for injector N1 were 0.62, 0.72, and 0.78 for $L_C/G = 10.5$, 18, and 33, respectively. Present results corresponding to the preceding results are 0.84, 0.87, and 0.90, respectively. One of the reasons for the higher value obtained by integration of the exit survey results may be the reaction occurring in the sampling probe, as pointed out by Mitani et al.[16,17] However, the effect of reaction in the probe on η_C would be small at $T_{tCi} = 2000$ K, as mentioned earlier.[17] The assumption of the constant gas properties in the calculation might be another reason for the discrepancy.

Effects of Wall-Injector Configuration

Figure 6 also shows the effects of the fuel-injector configurations indicated in Fig. 2 and Table 1, including the sweep angle of the orifice raw, Λ, and the constant-area length between the orifice raw and the diverging section, L_1. While η_C of the fuel injectors with a shorter constant-area length, namely, N2 and N3, are 1–6% higher than the other injectors, the η_{KEC} of them are slightly lower than those of N1, S1, and S2. As a result, there were no significant differences in K_C of all the injectors used in the present test of combustor no. I, namely, K_C for N2 injector was only 1–2.5% higher than those for the other injectors at $L_C/G = 18$.

Estimate of Loss Caused by Heat Release

Data of η_C and η_{KEC} of combustor no. I are summarized in Fig. 7. The data of five injectors are well correlated on a curve. As expected from Rayleigh flow analysis, η_{KEC} decreases as η_C increases. Combustion that occurred in the present supersonic combustors were neither constant-pressure (Brayton) nor constant-area (Rayleigh) processes. However, losses caused by heat release in these simplified processes can be analytically calculated,[1,5] and the results of such a calculation may be helpful to see the qualitative tendency. For the same value of η_C, because of its lower Mach number, the Rayleigh flow results in a slightly higher η_{KEC} than the Brayton process. For the present entrance conditions of combustor no. I, thermal choke of the Rayleigh flow occurs at about $\eta_C = 0.3$, whereas the Brayton process has no such limitation. Thus, a $\eta_{KEC} - \eta_C$ curve of the Brayton process for combustor no. I was calculated from Eq. (6), and it is shown as a solid curve in Fig. 7. The variable ω in Eq. (6) was equated to $1/(1+f)$, to exclude the effects of drag and axial momentum of fuel injection.[5] The trend of the experimental data is similar to the Brayton process curve, but the experimental results are higher than the solid curve. As shown in Fig. 3, a rather strong precombustion shock was produced for the $\varphi = 1$ case, and the flow in the constant-area duct downstream of the fuel injector, where the significant heat release occurred, may be decelerated to subsonic. η_{KEC} for the normal shock and the following subsonic constant-pressure combustion was calculated from Eq. (6) and the normal shock relation, and was shown by the dashed curve in Fig. 7. The dashed curve is closer to the experimental data than the solid curve. At the higher end of η_C, the experimental data showed an increase of loss, which was mainly a result of the friction at the combustor wall.

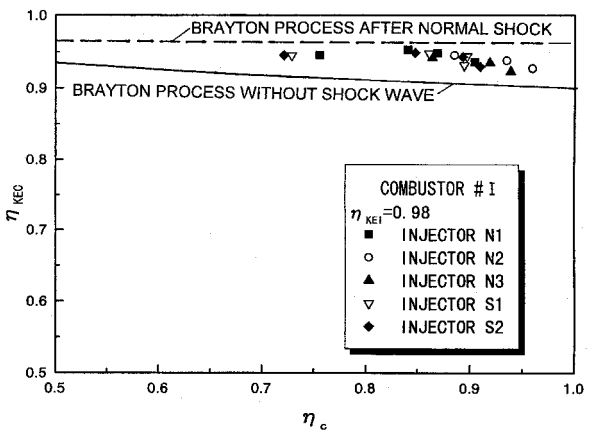

Fig. 7 Relation between η_C and η_{KEC} (combustor no. I).

Effects of Upstream Disturbance and Injection Angle

Figure 8 shows the test results of combustor no. II conducted at $M_\infty = 5.54$. To avoid a change of the upstream condition by the strong precombustion shock propagation inside the facility nozzle, φ_{total} was set to be 0.4. The two-dimensional arrowhead-shaped fuel-injection strut was placed at the middle plane of the combustor. Strut E with a blunt leading edge produced larger separation regions and a higher disturbance than strut A with a sharp leading edge.[14]

The values of η_C of struts A and E almost linearly increased with $\varphi_{per}/\varphi_{total}$. Strut E brought about a 15% higher η_C than strut A, except for $\varphi_{per}/\varphi_{total} = 1$, where η_C of strut E was saturated because the fuel was completely reacted, whereas η_C was less than unity because of heat loss to the walls. When $\varphi_{per}/\varphi_{total} = 0$, η_{KEC} of strut A was about 5% higher than that of strut E. It is clear that the strong shock wave produced by strut E reduced η_{KEC} of the flow without combustion. However, η_{KEC} of strut A reduced as $\varphi_{per}/\varphi_{total}$ increased, whereas η_{KEC} of strut E was effectively kept constant. η_{KEC} of both struts were nearly the same for $\varphi_{per}/\varphi_{total} = 1$. Because strut A produced a lower disturbance and less decelerate airstream than strut E, combustion with strut A occurred in a higher Mach number and resulted in a larger loss for heat addition.

The values of η_{KEC} for combustor no. II was considerably lower than those for combustor no. I. Because the experimental conditions of the two combustors were different, it was not possible to identify its reasons clearly. However, the drag of the strut might be one of the reasons for such a difference of η_{KEC} in the two combustors.

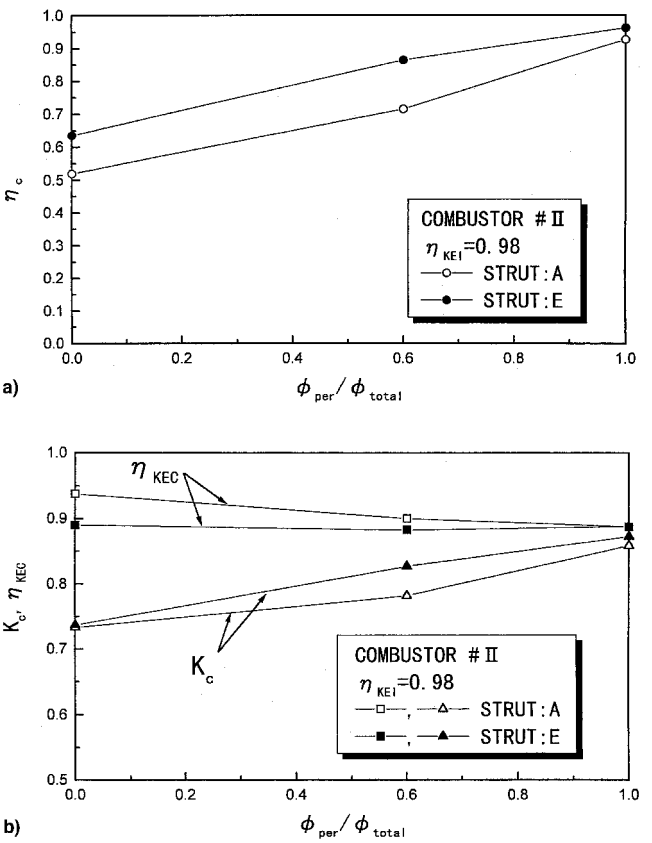

Fig. 8 Effects of disturbance and injection angle on scramjet combustor performances (combustor no. II): a) η_C and b) η_{KEC} and K_C.

The values of C_C and κ_∞ for combustor no. II were 5.25 and 5.26, respectively. For $\varphi_{per}/\varphi_{total} = 0$, strut A had 5% higher η_{KEC} and 12% lower η_C compared with those of strut E. They canceled each other and resulted in almost the same value of K_C for struts A and E. Increasing $\varphi_{per}/\varphi_{total}$ to 0.6, a 2% higher η_{KEC}, and a 15% lower η_C of strut A yielded a 4.5% lower K_C than that of strut E. For $\varphi_{per}/\varphi_{total} = 1$, η_{KEC} of both struts became nearly the same, and a 3.5% lower η_C of strut A resulted in a 1.5% lower K_C.

Blunt strut E had a higher K_C for the three $\varphi_{per}/\varphi_{total}$ values tested. These results indicate that a strong shock wave produced by duct geometry could enhance combustion and provide high thrust at a low Mach number regime for the scramjet engine, unless such a shock wave caused the combustor–inlet interaction or unstart of the inlet.

Conclusions

The scramjet combustor performance parameter K_C formulated in terms of η_{KEC} and η_C was evaluated with available data of direct-connect tests. The ideal nozzle exit properties were calculated from the measured data at the exit of two supersonic combustors with several different injector configurations, using the simulated flight conditions obtained from the combustor inlet conditions, and the performance parameter was derived from them.

1) The properties of the test gas supplied to the combustor inlet should be used for proper estimation of the simulated flight conditions.

2) η_{KEC} of combustor no. I with the wall injection was as high as 0.92–0.95 for $M_\infty = 6.93$ and $\varphi = 1$. η_{KEC} of combustor no. II with the strut injection for $M_\infty = 5.54$ and $\varphi = 0.4$ was 0.02–0.04 lower than that of combustor no. I.

3) The change of K_C of the present data was qualitatively similar to that of η_C, but not with η_{KEC}, because the heat of combustion was larger than the kinetic energy of the airstream and the change of η_C was much larger than that of η_{KEC}.

4) There was an optimum combustor length L_C/G, where K_C became the maximum because the increase of η_C with the length is canceled out by a decrease of η_{KEC}. The optimum L_C/G for combustor no. I was estimated as 15–20, which was about a half of the length required for sufficient mixing.

5) η_C and η_{KEC} of combustor no. I with the different injectors were well correlated, whereas those of combustor no. II with the different strut were not well correlated in the low η_C region because the different aerodynamic loss of struts became evident as the effect of combustion diminished.

Acknowledgments

Presented as Paper 97-7128 at the AIAA 13th International Symposium on Air Breathing Engines, Chattanooga, TN, Sept. 7–12, 1997. The authors are grateful to N. Chinzei, T. Mitani, K. Takita, and K. Takahashi for their discussion on this paper.

References

[1]Shapiro, A. H., *The Dynamics and Thermo-Dynamics of Compressible Fluid Flow*, Vol. 1, Ronald, New York, 1953, pp. 219–262.

[2]Swithenbank, J., Eames, I., Chin, S., Ewan, B., Yang, Z., and Zhao, X., "Turbulent Mixing in Supersonic Combustion System," AIAA Paper 89-0260, Jan. 1989.

[3]Billig, F. S., and Van Vie, D. M., "Efficiency Parameters for Inlets Operating at Hypersonic Speeds," *Proceedings of the 8th International Symposium on Air Breathing Engines*, AIAA, Washington, DC, 1987, pp. 118–130.

[4]Curran, E. T., Leingang, J., Carreiro, L., and Petters, D., "Review of Kinetic Energy Methods in High Speed Engine Cycle Analysis," 10th International Symposium on Air Breathing Engines, Paper 91-10.5(L), Nottingham, England, UK, Sept. 1991.

[5]Masuya, G., "Scramjet Performance Analysis with Simple Theories," *Journal of the Japan Society for Aeronautical and Space Sciences*, Vol. 43, No. 498, 1995, pp. 423–430 (in Japanese).

[6]Contensou, P., Marguet, R., and Huet, C., "Etude Theorique et Experimentale d'un Statoreacteur a Combustion Mixte (Domaine de vol Mach 3,5/7)," *La Recherche Aerospatiale*, No. 1973-5, 1973, pp. 259–274.

[7]Hoose, K. V., "Combustor Kinetic Energy Efficiency Analysis of the Hypersonic Research Engine Data," AIAA Paper 94-2818, June 1994.

[8]Murthy, S. N. B., and Czysz, P., "Energy Analysis of High Speed Vehicle Systems," AIAA Paper 90-0089, Jan. 1990.

[9]Riggins, D. W., McClinton, C. R., Rogers, R. C., and Bittner, R. D., "Investigation of Scramjet Injection Strategies for High Mach Number Flows," *Journal of Propulsion and Power*, Vol. 11, No. 3, 1995, pp. 409–418.

[10]Riggins, D. W., McClinton, C. R., and Vitt, P. H., "Thrust Loss in Hypersonic Engines Part 1: Methodology," *Journal of Propulsion and Power*, Vol. 13, No. 2, 1997, pp. 281–287.

[11]Riggins, D. W., "Evaluation of Performance Loss Methods for High-Speed Engines and Engine Components," *Journal of Propulsion and Power*, Vol. 13, No. 2, 1997, pp. 296–304.

[12]Chinzei, N., Komuro, T., Kudou, K., Murakami, A., Tani, K., Masuya, G., and Wakamatsu, Y., "Effects of Injector Geometry on Scramjet Combustor Performance," *Journal of Propulsion and Power*, Vol. 9, No. 1, 1993, pp. 146–152.

[13]Murakami, A., Komuro, T., and Kudou, K., "Experiment on a Rectangular Cross Section Scramjet Combustor (II)—Effects of Fuel Injector Geometry," National Aerospace Lab., TR-1220, Tokyo, Japan, Dec. 1993 (in Japanese).

[14]Masuya, G., Komuro, T., Murakami, A., Shinozaki, A., Nakamura, A., Murayama, M., and Ohwaki, K., "Ignition and Combustion Performance of Scramjet Combustors with Fuel Injection Struts," *Journal of Propulsion and Power*, Vol. 11, No. 2, 1995, pp. 301–307.

[15]Murakami, A., Komuro, T., Kudou, K., Masuya, G., and Chinzei, N., "An Air Heater for Scramjet Test," National Aerospace Lab., TR-912, Tokyo, Japan, Sept. 1986 (in Japanese).

[16]Mitani, T., Hiraiwa, T., Sato, S., Tomioka, S., Kanda, T., and Tani, T., "Comparison of Scramjet Engine Performance in Mach 6 Vitiated and Storage Heated Air," *Journal of Propulsion and Power*, Vol. 13, No. 5, 1997, pp. 635–642.

[17]Mitani, T., Chinzei, N., and Masuya, G., "Experiment on Reaction Quenching in Gas Sampling Probes for Scramjet Engine Testing," *27th Symposium (International) on Combustion*, The Combustion Inst., Pittsburgh, PA, 1998, pp. 2151–2156.

[18]Schlichting, H., *Boundary Layer Theory*, 7th ed., McGraw–Hill, New York, 1979, pp. 330–333.

[19]Northam, G. B., and Anderson, G. Y., "Supersonic Combustion Ramjet Research at Langley," AIAA Paper 86-0159, Jan. 1986.